One-Bit Constrained Measurements of Parametric Signals

Paolo Carbone, *Fellow, IEEE*, Johan Schoukens, *Fellow, IEEE*, Alessio De Angelis, *Member, IEEE*, Antonio Moschitta, *Member, IEEE*, and Francesco Santoni, *Member, IEEE*

***Abstract*— This article introduces a novel estimation framework for the parameters in a linear-in-the-parameter estimation problem when one-bit measurements are processed. We consider a periodic signal, whose components have unknown amplitudes and phases. This signal is assumed to be quantized by a single comparator under various problem settings. To provide enough information for the estimation of the signal parameters based on one-bit quantized signal measurements, the threshold in the one-bit comparator is assumed known. Several problem settings are considered. They include synchronous/asynchronous sampling, presence or absence of deterministic or stochastic dither, and presence or absence of additive noise. The results obtained by applying three alternative methods are compared and analyzed. Experimental results on a two-component 1.2-GHz signal validate the theoretical analysis. It is shown that several estimation approaches are available, which provides different performance levels, in terms of final estimation accuracy and computational complexity.**

***Index Terms*— Estimation, identification, nonlinear estimation problems, nonlinear quantizers, quantization.**

I. Introduction

MEASUREMENT of signals that depend linearly on unknown parameters is a common problem in electrical engineering. As an example, this occurs in system identification when the user records system input and output signals to apply model identification methods [1]. Similarly, the amplitudes and phases of the components of a periodic signal are of interest when, e.g., synchrophasors must be measured in a power distribution network [2]. The possibility to perform measurement and estimation of the unknown signal parameters using simple approaches based on a minimum hardware setup can lead to new applications, ease hardware complexity, and reduce design costs by transferring complexity from the hardware to the software domain.

In this article, we demonstrate how to estimate the amplitudes and phases of a periodic signal based on binary data obtained through a comparator. This problem was the object of several studies dating back to [3], where the problem of reconstructing an analog signal from its binary quantized version is analyzed, and to [4], where the effect of quantization for estimation and control purposes was analyzed. It was further considered in [5] and [6] under the assumption of known and unknown probability density function (PDF) of the noise affecting the quantizer input and acting as a dither signal [7] and solved using a maximum-likelihood estimator (MLE). In [8], estimates of multivariate signal parameters are obtained under the assumption of dependent noise affecting the processed one-bit quantized data. An MLE is used and theorems are proved about the normality and consistency of the proposed statistics. In [9], a technique is illustrated for channel estimation using Gaussian corrupted piloting signals quantized using a 1-bit analog-to-digital converter (ADC). An MLE-based approach is described along with a maximum *a posteriori* probability estimator.

Processing of binary data for estimation purposes was also extensively covered in the area of signal processing [10]–[13], telecommunications [14], radar signal processing [15]–[17], and one-bit compressive sensing [18]–[20]. The idea of joining standard ADC architectures based on a binary quantizer, with embedded estimation methods, is also a recent research topic [21]–[24]. Motivation and a theoretical foundation for one-bit estimation can be found in [25]. A variety of methods and problem settings for system identification based on quantized data can be found in [26], while Wang *et al.* [27] introduced a unifying approach. Finally, Saito *et al.* [28] and Carbone *et al.* [29] discussed the usage of Bussgang's theorem [30] in the context of multiantenna receivers and one-bit system identification, respectively.

This article illustrates a novel estimation framework that enables processing of binary data under several problem settings, possibly including dither and noise sequences. The illustrated estimators are based on constrained optimization, following the ideas described in [31] and [32]. Three estimation approaches are introduced, which process binary data to provide estimates of a linear-in-the-parameter periodic signal. The considered problem settings include the presence of known/unknown deterministic and stochastic dither samples and wideband noise. Monte Carlo simulations and experimental results validate the proposed techniques and prove their applicability when high-frequency periodic signals are sampled and quantized by a simple comparator.

II. Problem Setup

In this article, we consider the estimation of the parameters of band-limited periodic signals expressed as a

Manuscript received 17 January 2022; revised 14 April 2022; accepted 26 May 2022. Date of publication 9 June 2022; date of current version 23 June 2022. This work was supported in part by the Ricerca di Base 2019 (1-Bit Signal Measurements) and in part by the Ricerca di Base 2020 (tecniche avanzate di stima parametrica e caratterizzazione di segnali e sistemi), University of Perugia. The Associate Editor coordinating the review process was Dr. John Lataire. *(Corresponding author: Paolo Carbone.)*

Paolo Carbone, Alessio De Angelis, Antonio Moschitta, and Francesco Santoni are with the Department of Engineering, University of Perugia, 06125 Perugia, Italy (e-mail: paolo.carbone@diei.unipg.it).

Johan Schoukens is with the Department INDI, Vrije Universiteit Brussel, 1050 Brussels, Belgium.

Digital Object Identifier 10.1109/TIM.2022.3181901

trigonometric polynomial

$$s(t) = \sum_{p=1}^{H} a_p \cos(2\pi pft) + \sum_{p=1}^{H} b_p \cos(2\pi pft) \tag{1}$$

where the coefficients a_p and b_p represent the amplitudes to be estimated, f is the known fundamental frequency, H is the number of harmonic components, and t is the time. It is further assumed that some of these components have amplitude 0 and need not be estimated. Define $\mathcal{P} = \{m_1, \ldots, m_P\}$ as the set of component indices whose corresponding amplitudes need to be estimated, and $P \leq H$ its cardinality. The signal (1) is input to a comparator to provide

$$s_q(t) = Q(s(t)) = \begin{cases} 1, & s(t) \leq T \\ -1, & \text{otherwise} \end{cases} \tag{2}$$

where T is the comparator's constant threshold. The problem addressed in this article is the following: the users collect binary discrete-time samples of $s_q(\cdot)$, knows $\mathcal{P}$, and wants to estimate the $2P \times 1$ vector $\Theta = [\theta_1, \ldots, \theta_{2P}]^T = [a_{m_1}, \ldots, a_{m_P}\ b_{m_1}, \ldots, b_{m_P}]^T$, of still unknown amplitudes.

III. Estimation Framework

The general estimation principle that exploits binary data to estimate the parameters of an otherwise unknown periodic signal is based in this article on the solution of constrained problems. Three estimation techniques will be analyzed and compared:

1) method 1, QUADPARAM, based on the numerical minimization of a quadratic cost function;
2) method 2, QUADSIGNAL, based on quadratic programming;
3) method 3, LINPARAM, based on linear programming.

All methods rely on constrained optimization. The setup of constraints depends on the particular problem setting. The following list includes settings that can be solved with the techniques described in this article:

1) type of sampling (asynchronous/synchronous);
2) presence of added dither to perform quantization (known deterministic dither, random dither with known PDF);
3) disturbances affecting quantization (random noise with known/unknown PDF).

Other settings can, in principle, be considered such as the number of components P or signal frequency f being unknown. These cases are excluded from the following analysis.

A. Signal Sampling and Preprocessing

By sampling (2) with a constant period T_C, such that $\lambda = fT_C$, we obtain a discrete-time sequence s_{qn}, $n = 0, \ldots, N-1$, where N is the number of collected samples. If λ is a rational number, synchronous sampling results, asynchronous sampling if λ is irrational. In the rest of this article, λ is assumed to be known. Because of the periodicity of the trigonometric functions, sampling of (1) for $n = 0, \ldots, N-1$ provides

$$s_n = s(nT_c) = \sum_{p=1}^{P} a_{m_p} \cos(2\pi m_p \langle n\lambda \rangle) + \sum_{p=1}^{P} b_{m_p} \cos(2\pi m_p \langle n\lambda \rangle) \tag{3}$$

where $\langle \cdot \rangle$ is the fractional part operator.

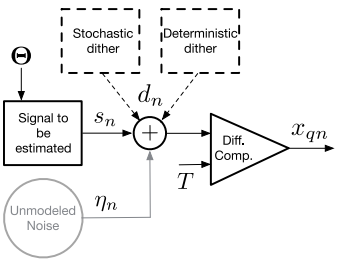

Fig. 1. Measurement framework considered in this article: estimation of the parameters Θ in a periodic signal, s_n, based on binary measurements, x_{qn}, when synchronous/asynchronous sampling is adopted under the possible presence of unmodeled noise (gray color), and the possible alternative presence of stochastic or deterministic dither sources. Solutions to the problems associated with the various settings are described in this article.

B. Discrete-Time Models

The samples of the signal to be measured can be represented as a vector $\mathbf{s} = [s_0, s_1, \ldots, s_{N-1}]^T$ or $\mathbf{s} = \mathbf{H}\Theta$, where the parameter vector $\Theta = [a_{m_1}, \ldots, a_{m_P}\ b_{m_1}, \ldots, b_{m_P}]^T$ is a $2P \times 1$ vector and $\mathbf{H}$ is an $N \times 2P$ matrix, whose nth row is $\mathbf{h}_n$, a $1 \times 2P$ vector. Under the noiseless case, each sample s_n, $n = 0, \ldots, N-1$ is quantized to provide $s_{qn} = Q(s_n)$ so that the $N \times 1$ vector $\mathbf{s}_q = [s_{q0}, s_{q1}, \ldots, s_{q(N-1)}]^T$ can be defined.

Some of the problem settings require modeling the presence of noise and dither. If η_n and d_n are the unknown and known noise and dither samples, respectively, define $x_{qn} = Q(s_n + \eta_n + d_n)$, and the corresponding $N \times 1$ vector $\mathbf{x}_q = [x_{q0}, x_{q1}, \ldots, x_{q(N-1)}]^T$. The sequence η_n may also represent random dither with known PDF, as explained in Section III-F. A scheme of the signal chain considered in this article is shown in Fig. 1 that illustrates the various estimation problem settings.

The application of the most suitable estimator requires knowledge of how the signal was sampled. Some of the estimation procedures described in the following exploit the principle of equivalent-time sampling (ETS) [33]. Two such methods are described in Sections III-C and III-D.

C. ETS When Sampling Is Synchronous

When sampling is synchronous, $\lambda = D/M$, where D and M are two irreducible natural numbers. Consider the map $\lambda_n = \langle n\lambda \rangle$, when $n = 0, \ldots, N-1$. The sequence λ_n represents the equivalent-time instants at which one period of (3) is sampled. When $N > M$, some of these values repeat, whereas when $N \leq M$, this map provides distinct values. If $D = 1$, samples s_n are already sorted in increasing time order and sequential ETS results. If $D > 1$, they must be first ordered to represent a single period of (1). Accordingly, a new sequence $\tilde{s}_m$,

$m = 0, \ldots, N-1$, is obtained by permuting samples in $\mathbf{s}$ so that they represent signal samples in increasing order of λ_n within a single period. Other theoretical details can be found in [34].

D. ETS When Sampling Is Asynchronous: Quasi-ETS

When sampling is asynchronous, λ is irrational and $\lambda_n = \langle n\lambda \rangle$ provides different samples for different values of n. Thus, ETS cannot be exploited since signal periodicity is not considered. However, its benefits can be approximated through quasi-ETS (QETS), introduced in [34]. Consider the map λ_n when $n = 0, \ldots, N-1$ [35]–[37]. The indices $n = 0, \ldots, N-1$ are partitioned in $E \gg 1$ subsets $\mathcal{I}_j$ such that

$$\mathcal{I}_j = \{n | j\epsilon \leq \lambda_n < (j+1)\epsilon\}, \quad j = 1, \ldots, E \tag{4}$$

where $\epsilon = (1/E) \ll 1$ is a user-defined value. Since P is finite, the first derivative of $s(t)$ is bounded in magnitude. Moreover, since $s(t)$ is a continuous function, it is always possible to find a value of ϵ such that points in a neighborhood of $j\epsilon$ in (4) are transformed in points in a neighborhood of the signal amplitude. Thus, indices in $\mathcal{I}_j$, for a given j, correspond approximately to the same sampled value, provided that ϵ is sufficiently small. To apply QETS, the partition of indices (4) must first be constructed and indices in $\mathcal{I}_j$ used to recover samples in s_n as if they referred to the same value. Observe that if ϵ is sufficiently small and synchronous sampling is adopted, partitioning of the time indices becomes equivalent to applying ETS, as explained in Section III-C.

E. Setup of the Solution Constraints: Noise-Free Deterministic Dither

When the acquisition is noise-free, the binary sequence directly induces a natural set of constraints on the estimated input signal $\hat{s}_n$. In fact, the comparator provides knowledge on the input signal being above or below the known threshold T. Thus, the estimator is constrained to search estimates $\hat{s}_n$, such that $\hat{s}_n \leq T$ if $s_{qn} = 1$ and $\hat{s}_n > T$ if $s_{qn} = -1$, when dithering is not applied. If known time-varying dither d_n is added, the corresponding constraints become $\hat{s}_n \leq T - d_n$, if $s_{qn} = 1$, and $\hat{s}_n > T - d_n$, if $s_{qn} = -1$.

F. Setup of the Solution Constraints: Noise-Free Random Dither

When random dither, η_j, having known PDF, is added to perform quantization, ETS or QETS can first be applied to preprocess data. When QETS is applied, preprocessing results in a partition of the time indices, as described in Section III-D.

By making the approximation that ϵ is sufficiently small, it is assumed that indices in $\mathcal{I}_j$, $j = 1, \ldots, E$, refer approximately to the same signal amplitude s_i. A mean value $\overline{s}_j = (1/|\mathcal{I}_j|) \sum_{n \in \mathcal{I}_j} s_n$, where $|A|$ is the cardinality of A, can then be defined. Correspondingly, $\overline{p}_j = (1/|\mathcal{I}_j|) \sum_{n \in I_j} (1/2)(x_{qn} + 1)$ approximately represents the probability of the event $\mathcal{E}_j = \{\overline{s}_j + \overline{\eta}_j \leq T\}$, where $\overline{\eta}_j = (1/|\mathcal{I}_j|) \sum_{n \in I_j} \eta_n$ is the average noise amplitude of samples in $\mathcal{I}_j$. Observe that $P(\mathcal{E}_j) \simeq \overline{p}_j \simeq F_\eta(T - \overline{s}_j)$, where $F_\eta(\cdot)$ is the dither cumulative distribution function (CDF).

The next step is to find an approximated confidence interval for $\overline{p}_j$. In the made assumption, $|\mathcal{I}_j| \overline{p}_j = \sum_{n \in I_j} (1/2)(x_{qn} + 1)$ is a binomial random variable with success probability in each trial approximately equal to $\overline{p}_j$ and number of trials $|\mathcal{I}_j|$. For $j = 1, \ldots, E$, the choice of a confidence level $0 < \alpha < 1$ results in the calculation of

$$L_j = F^{-1}(\alpha/2, |\mathcal{I}_j|, \overline{p}_j), \quad U_j = F^{-1}(1 - \alpha/2, |\mathcal{I}_j|, \overline{p}_j) \tag{5}$$

such that $P(L_j < |\mathcal{I}_j| \overline{p}_j < U_j) \simeq 1 - \alpha$, where $F^{-1}(\beta, N, \pi)$ is the inverse CDF of a binomial random variable with N trials and π as success probability, calculated in $0 \leq \beta \leq 1$. When the user chooses a small value for α

$$\frac{L_j}{|\mathcal{I}_j|} < \overline{p}_j < \frac{U_j}{|\mathcal{I}_j|} \tag{6}$$

can be considered a hard constraint on $\overline{p}_j$. This constraint finally results in a corresponding hard constraint on $\overline{s}_j$ to be included in the problem solution setup. By recalling that $\overline{p}_j \simeq F_\eta(T - \overline{s}_j)$, from (6), we have

$$l_j = T - F_\eta^{-1}\left(\frac{U_j}{|\mathcal{I}_j|}\right) < \overline{s}_j < T - F_\eta^{-1}\left(\frac{L_j}{|\mathcal{I}_j|}\right) = u_j \quad j = 1, \ldots, E \tag{7}$$

where $F_\eta^{-1}(\cdot)$ represents the dither inverse CDF.

Observe that if U_j or L_j is equal to $|\mathcal{I}_j|$ or 0, the dither CDF in (7) might not be invertible. Accordingly, the corresponding constraint is dropped from further processing and the confidence interval may become one sided or even can be dropped entirely. Thus, only a subset $\mathcal{S}$ of all possible E indices might result in applicable constraints. By approximating

$$\overline{s}_j \simeq \overline{\mathbf{h}}_j \Theta, \quad j \in \mathcal{S} \subseteq \{1, 2, \ldots, E\} \tag{8}$$

where the $1 \times 2P$ vector $\overline{\mathbf{h}}_j$ is given by

$$\overline{\mathbf{h}}_j \simeq \frac{1}{|\mathcal{I}_j|} \sum_{i \in \mathcal{I}_j} \mathbf{h}_i \tag{9}$$

it can be written $\overline{\mathbf{s}} \simeq \overline{\mathbf{H}} \Theta$, where the $|\mathcal{S}| \times 1$ vector $\overline{\mathbf{s}} = [\overline{s}_1, \overline{s}_2, \ldots, \overline{s}_{|\mathcal{S}|}]^T$ and $\overline{\mathbf{H}}$ is the reduced $|\mathcal{S}| \times 2P$ matrix, with rows $\overline{\mathbf{h}}_j$, $j \in \mathcal{S}$.

The estimator introduced in Section IV-E1 will search feasible values for the parameters in (8) so that constraints (7) are satisfied. Because of the made approximations and of the assumption on (7) being hard constraints, a feasible solution might not be found. In this case, the user may relax the constraints by decreasing the value of α in (5).

Fig. 2 shows the working principle of QETS, along with the indication of the constraint intervals, using red segments that are, in some cases, open-ended. This approach will tolerate modeling uncertainties, such as due to imperfect knowledge of the added dither PDF or due to other unmodeled disturbances.

Observe that the choice of the added dither variance is the result of a compromise. Dither allows samples that are far from the quantizer's threshold to possibly cross the threshold. Crossing probability depends on how distant the samples are

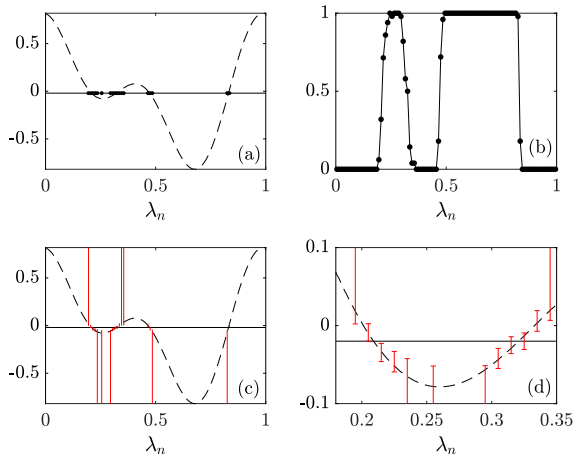

Fig. 2. One period of a two-component periodic signal acquired by a one-bit quantizer with threshold $T = -0.02$, indicated in (a), (c), and (d). Zero-mean Gaussian dither with $\sigma = 0.0225$ is assumed and $N = 5000$ samples collected and processed. An irrational value for $\lambda = 0.18132\ldots$ is set, with λ_n representing the ETS variable. By processing data as explained in Section III-F, QETS is implemented using $\epsilon = 0.01$ that results in $E = 100$ subintervals of the $[0, 1)$ equivalent-time period. (a) Noiseless original signal; dots represents the indices $j \in \mathcal{S}$ for which $0 < \overline{p}_j < 1$. (b) Estimated probabilities $\overline{p}_j$ are obtained by processing the one-bit quantized sequence as detailed in Section III-F. (c) Each of these probabilities is used to estimate confidence intervals expressed in (7) when assuming $\alpha = 0.01$. These are graphed using red vertical lines. (d) Expanded view. The estimator provides a solution resulting in a reconstructed signal, shown using dashed lines, intercepting all intervals, acting as problem solution constraints. Observe that some of the red-colored intervals are one sided, because of the lack of invertibility of the dither CDF in (7) when calculating l_j and u_j. In fact, when the signal is close to the threshold, because of the noise span, $\overline{p}_j$ is more likely not to result in 0 or 1.

from the threshold and on the dither magnitude. Thus, for any given sample, larger dither variance results in a larger probability of the samples to cross the threshold and to provide information useful for estimation purposes. At the same time, the dither variance affects the variance with which the crossing probability $\overline{p}_j$ is estimated. The effect of added noise used as dither in the estimation of sinewave parameters is further discussed in [34].

G. Setup of the Solution Constraints: Noisy Case

When additive noise affects the acquisition process, constraints can be set up as in the noise-free case. However, a tolerance value $\delta > 0$, considered as the maximum noise magnitude, can be programmed in the solver of the optimization problem, to consider the constraint satisfied, if the constraint violation is less than δ in magnitude. Alternatively, the estimation can be performed by a suitable choice of the cost function, as explained in Section IV-A3, which explains the usage of the QUADSIGNAL estimator. Finally, if the noise PDF is known, noise can be regarded as stochastic dither and the estimation problem can still be solved by adopting the applicable solver as described in Sections III-F and IV-E1.

H. Role of the Threshold Value T

The output binary sequence must be enough informative to allow estimation. As an example, if T is larger than the maximum value in $s(t)$, s_q will always be equal to 1 and estimation will not be possible. The additional assumption is made that $T \neq 0$. In fact, when $T = 0$, binary quantization does not return enough information for the estimation of the amplitudes of the signal components when dithering is not applied. When $P = H$, it is known that the number of roots in one period of the trigonometric polynomial $s(t) - T$ is, in the complex domain, $2P$ [38].

The choice of T results in some or in all of these roots to be real-valued. Neglecting the possible multiplicity of solutions, when $P = H$ and all roots of $s(t) - T$ are real-valued, T intercepts a single period of $s(t)$ in $2P$ distinct values $t_1, \ldots, t_{2P}$ when $t \in [0, (1/f))$. Under these assumptions, if these crossing times were exactly known, the estimation problem could be solved without approximations through a system of equations. In practice, the binary output provides constraints that result in lower and upper bounds for each t_i, that is, no longer exactly known. The estimation framework described in this article solves this problem.

When $P = H$, if some of the roots $t_1, \ldots, t_{2P}$ are complex-valued, T intercepts a single period of $s(t)$ in fewer than $2P$ distinct crossing times. With the need to estimate $2P$ parameters, this setting results in a number of degrees of freedom for the value of the unknown parameters that hold even if crossing times were known exactly. By also considering the additional uncertainty due to constraints, consistent estimation of all parameters becomes unfeasible. By processing the signal binary output, it is possible to check the number of crossing times under the noiseless signal assumption or under large signal-to-noise ratio (SNR) conditions.

When noise or dither affects quantization, the probability of having less than the $2P$ equations needed to avoid this problem can be controlled by the magnitude of the dither that can be made larger to increase the probability of samples crossing the threshold when knowing the noise PDF.

IV. Estimators

The detailed constrained estimation approaches are described in this section. They are classified according to whether additive noise affects or does not affect quantization, while the type of sampling does not affect the estimation principles. The descriptions include the cases when deterministic or random dither is assumed. The following describes the estimation framework under the considered problem settings.

A. No Noise, No Dither Setting

1) Theory: While the absence of assistive signals during quantization makes this problem the hardest to solve, signal estimation is still possible, as done, e.g., in [39]. Estimation can be performed by setting the problem as a constrained minimization problem. In fact, each element in $\mathbf{s}_q$ informs the user about the corresponding sample in $\mathbf{s}$ being below or above the threshold T. Thus, any feasible solution for Θ must satisfy these constraints. Three methods are described in this section. The first one is based on the minimization of a cost function calculated from the measurement data. In the second one, the cost function includes the estimation of each signal sample before quantization. The third approach uses linear programming to explore the region of feasible parameter values.

2) Method 1—QUADPARAM: If a quadratic cost function is selected, the minimization problem providing estimates of Θ can be setup as follows:

$$\hat{\Theta} = \arg\min_{\Theta} \frac{1}{N}\sum_{n=0}^{N-1}(s_{qn} - \mathbf{h}_n\Theta)^2 \quad \text{s.t. } s_n \le T, \quad \text{if } s_{qn} = 1 \text{ or } s_n > T, \text{ if } s_{qn} = -1 \tag{10}$$

that can equivalently be written as

$$\hat{\Theta} = \arg\min_{\Theta} \frac{1}{N}(\mathbf{s}_q - \mathbf{H}\Theta)^T(\mathbf{s}_q - \mathbf{H}\Theta) \quad \text{s.t. } \operatorname{diag}(\mathbf{s}_q)\mathbf{H}\Theta \preccurlyeq T\mathbf{s}_q \tag{11}$$

where $\operatorname{diag}(\mathbf{s}_q)$ is an $N \times N$ matrix, whose principal diagonal contains the elements in $\mathbf{s}_q$, and $\preccurlyeq$ means componentwise inequality between two vectors. Efficient algorithms exist to solve (11), such as the interior-point technique [40], [41] implemented, e.g., by `fmincon` in MATLAB that provides quick solutions for problems with N in the order of 10^4. This estimator requires the output sequence to be sufficiently informative about the input signal. The value of T strongly influences this condition, as explained in Section III-H.

3) Method 2—QUADSIGNAL: An alternative method can be obtained by adapting the technique described in [42] and [43]. First, the following constrained minimization problem is setup:

$$\hat{\Theta} = \arg\min_{(\mathbf{s},\Theta)} \frac{1}{N}\sum_{n=0}^{N-1}(s_n - \mathbf{h}_n\Theta)^2 \quad \text{s.t. } s_n \le T, \quad \text{if } s_{qn} = 1 \text{ or } s_n > T, \text{ if } s_{qn} = -1. \tag{12}$$

Notice that, with respect to (10), this cost function involves s_n and not s_{qn}. It can be rewritten as [42], [43]

$$\begin{aligned}\frac{1}{N}\sum_{t=1}^{N}(s_n - \mathbf{h}_n\Theta)^2 &= \frac{1}{N}(\mathbf{s} - \mathbf{H}\Theta)^T(\mathbf{s} - \mathbf{H}\Theta) \\ &= \frac{1}{N}\begin{bmatrix}\Theta^T & \mathbf{s}^T\end{bmatrix}\begin{bmatrix}\mathbf{H}^T\mathbf{H} & -\mathbf{H}^T \\ -\mathbf{H} & \mathbf{I}_N\end{bmatrix}\begin{bmatrix}\Theta \\ \mathbf{s}\end{bmatrix} \\ &\triangleq \frac{1}{N}\mathbf{Y}^T\mathbf{Z}\mathbf{Y}\end{aligned} \tag{13}$$

where $\mathbf{I}_N$ is the $N \times N$ identity matrix [43]

$$\mathbf{Y} = \begin{bmatrix}\Theta \\ \mathbf{s}\end{bmatrix}, \quad \mathbf{Z} = \begin{bmatrix}\mathbf{H}^T\mathbf{H} & -\mathbf{H}^T \\ -\mathbf{H} & \mathbf{I}_N\end{bmatrix}. \tag{14}$$

Thus, the following quadratic programming problem can be setup:

$$\hat{\mathbf{Y}} = \arg\min_{\mathbf{Y}} \frac{1}{N}\mathbf{Y}^T\mathbf{Z}\mathbf{Y} \quad \text{s.t. } \mathbf{A}\mathbf{Y} \preccurlyeq \mathbf{Y}_U \tag{15}$$

where

$$\mathbf{Y}_U = \begin{bmatrix}\Theta_U \\ \mathbf{S}_U\end{bmatrix} \tag{16}$$

Θ_U is assumed as a prior upper bound for Θ, $\mathbf{S}_U = T\mathbf{s}_q$, and

$$\mathbf{A} = \left[\begin{array}{c|c}\mathbf{I}_{2P} & \mathbf{0} \\ \hline \mathbf{0} & \operatorname{diag}(\mathbf{s}_q)\end{array}\right] \tag{17}$$

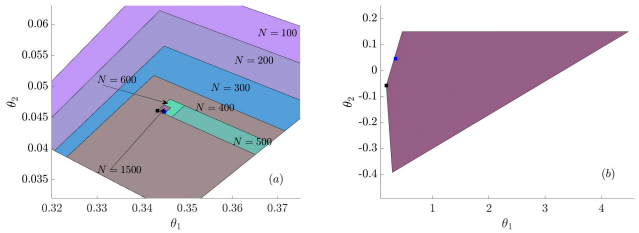

Fig. 3. Feasible regions in the estimation of the two parameters of a single sinusoids, quantized using a noise- and dither-free comparator with $T = 0.15$ when N takes the values indicated in (a). (a) Asynchronous sampling with $\lambda = 0.11323\ldots$ (b) Synchronous sampling case with $\lambda = 0.2$. Blue and black squares refer to the true and estimated parameters using QUADPARAM, respectively. In (a), the regions shrink about the true values when N increases and sampling is asynchronous. Conversely, in (b), the feasible regions overlap and do not depend on N.

with $\mathbf{I}_{2P}$ as the $2P \times 2P$ identity matrix. Efficient procedures exist to solve quadratically constrained problems, such as the interior-point-convex method [44], implemented by, e.g., `quadprog` in MATLAB.

4) Method 3—LINPARAM: It is expected that regardless of the cost function, the set of inequalities in the constraints alone will result in a feasible region for the searched parameters. It can be observed that when sampling is asynchronous, by increasing N, λ_n uniformly fills the [0, 1) interval according to Weyl's equidistribution theorem [45]. Accordingly, the feasible region increasingly shrinks around the true sets of parameters. Conversely, if sampling is synchronous, region shrinking does not occur when N increases. However, constraints still provide boundaries of a feasible region for the searched parameters.

As an example, consider the case of a single sinusoid with $a_1 = 0.3449\ldots$ and $b_1 = 0.0459\ldots$ The sinusoid is sampled either asynchronously with $\lambda = 0.11323\ldots$ or synchronously with $\lambda = 0.2$ and quantized by a comparator with $T = 0.15$. When no dither is employed and quantization is noise-free, the shapes of the feasible regions are shown in Fig. 3(a) and (b) under the asynchronous and synchronous sampling assumptions, respectively. The number of processed samples takes values in $[1, 2, 3, 4, 5, 6, 7, 15] \cdot 10^2$, in both cases. The position of Θ is indicated by a blue square, while the estimate provided by QUADPARAM is indicated by a black square. It can be observed that the region shrinks around the true parameters when sampling is asynchronous and N is increased. Conversely, the regions overlap when N is increased and synchronous sampling is adopted.

By randomly selecting 10^3 sets of parameters within the feasible region associated with $N = 500$, the envelope of all single-period reconstructed sinewaves is shown in Fig. 4. All sinewaves within the envelope are based on parameters obeying the constraints. The choice of a cost function to be minimized forces the selection of one among them.

A canonical linear programming problem can be setup to solve a set of minimization problems that share the same sets of constraints, but different cost functions are chosen to explore the boundaries of the feasible region for each parameter. As an example, for each $j = 1, \ldots, 2P$, the two following linear programming problems can be setup, for a

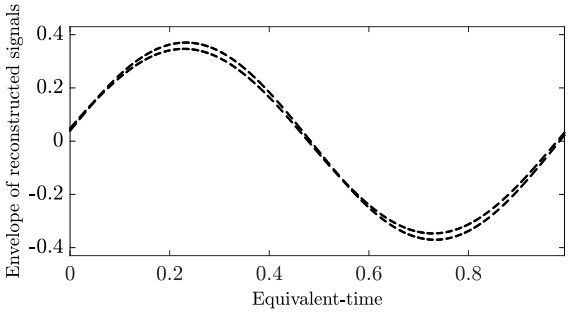

Fig. 4. Envelope of minimum and maximum values of the reconstructed sinewaves, with parameters within the feasible region, associated with $N = 500$ in the same example as in Fig. 3. The two graphs are obtained by processing 10^3 sets of parameters, randomly chosen within the feasible region.

TABLE I

VALUES OF THE SIMULATION PARAMETERS. FUNDAMENTAL FREQUENCY SET AT THE VALUE $\lambda = 0.011323235562$

Component	Harmonic index	Amplitude	Phase (rad)
1	1	0.348	0.1324
2	3	0.2	0.2
3	7	0.251	0.3
4	9	0.3	0.123
5	11	0.2	3

total of $2P$ problems:

$$\hat{\theta}_j^+ = \arg\min_{\Theta} \theta_j \quad \text{s.t. } \text{diag}(\mathbf{s}_q)\mathbf{H}\Theta \preccurlyeq T\mathbf{s}_q \tag{18}$$

and

$$\hat{\theta}_j^- = \arg\min_{\Theta}(-\theta_j) \quad \text{s.t. } \text{diag}(\mathbf{s}_q)\mathbf{H}\Theta \preccurlyeq T\mathbf{s}_q. \tag{19}$$

These solutions provide bounds for the maximum and minimum values in the estimate of θ_j. A single estimated value may be selected by choosing, e.g., their mean value $\hat{\theta}_j = 1/2(\hat{\theta}_j^+ + \hat{\theta}_j^-)$. After each $\hat{\theta}_j$ is calculated, an estimate of Θ is achieved. The simplex algorithm can be used to solve (12) and (18) [44].

5) Simulation Results: A fifth-harmonic component periodic signal is considered in this article with parameters' values specified in Table I. Define $s_n(h) = \sin(2\pi n \cdot h\lambda)$ and $c_n(h) = \cos(2\pi n \cdot h\lambda)$, where λ is the normalized frequency, n is the time index, and h is the harmonic index. Furthermore, define $\mathbf{H}$ as in (20), shown at the bottom of the page. Consider that $P = 5$, $\Theta = [\theta_1, \theta_2, \ldots, \theta_{10}]^T$, and $\mathbf{s} = \mathbf{H}\Theta$. By chosing $\lambda = 0.011323235562$ and $N = 2500$, the equivalent-time signal sequence is shown in Fig. 5. Samples in $\mathbf{s}$ are graphed after permuting the time indices so to obtain a single signal period. The permutation is performed by sorting in increasing order the time sequence $\lambda_n = \langle n\lambda \rangle$, $n = 0, \ldots, N-1$. Sorting provides a new sequence of permuted equivalent-time values $\lambda_{(n)}$ that is used to plot all data in this article.

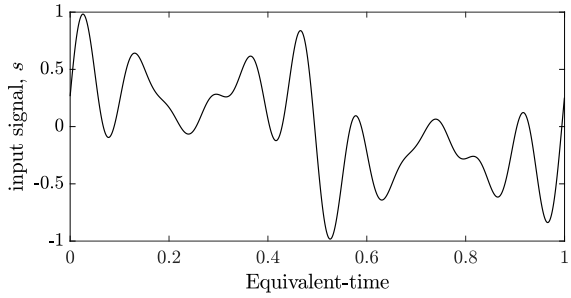

Fig. 5. One period of a five-component noiseless periodic signal based on $\mathbf{H}$ defined in (20). $N = 2500$ equivalent-time indices are obtained by sorting the sequence $\lambda_n = \langle n\lambda \rangle$, $n = 0, \ldots, N-1$ in increasing order and by accordingly reordering the time indices (see the text). Table I shows the used signal components, with $\lambda = 0.011323235562$.

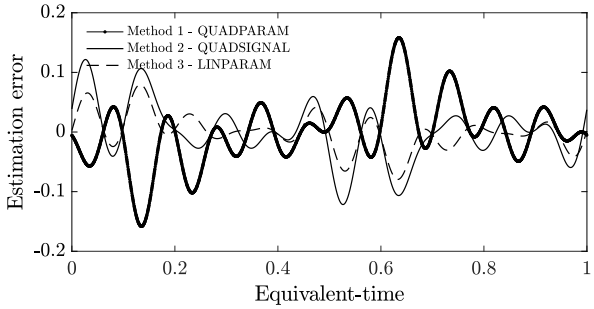

Fig. 6. No noise, no dither setup: estimation error in the case of the signal with components listed in Table I. $N = 2500$ equivalent-time values are processed by sorting the sequence $\lambda_n = \langle n\lambda \rangle$ in increasing order (see the text). Results of all methods are shown when $T = -0.1643\ldots$

Results obtained by processing $\mathbf{s}_q$ are shown in Figs. 6 and 7. Fig. 6 shows one period of the estimation errors associated with the usage of all three methods. Results obtained by varying the threshold T in $(-0.2, 0.2)$ are shown in Fig. 7, where the L^2-norm of these errors is graphed normalized to N. This figure also shows that when T is close to 0, the error provided by all estimators increases largely, as expected. In fact, when $T = 0$, information about the amplitudes of the signal components is lost since the output sequence becomes insensitive to multiplication factors applied to the input signal. Thus, the value of T influences the estimator performance.

Observe also that estimation accuracy is influenced by the periodicity of the sequence in $\mathbf{s}_q$. For instance, when λ is a rational number (D/M), D and M do not share common dividers, and $N > M$, $\mathbf{s}_q$ contains repeated samples. Consequently, increasing N will not result in better estimation accuracy. Conversely if $N < M$ or when λ is an irrational number, increasing N will improve estimation accuracy.

To show the accuracy with which parameters are estimated when N increases, the differences $\hat{\theta}_j^+ - \hat{\theta}_j^-$, $j = 1, \ldots, 2P$, with definitions in (18) and (19) are evaluated. Results are shown in Fig. 8. When asynchronous sampling is adopted, increasing N results in signal samples that are closer to the

$$\mathbf{H} = \begin{bmatrix} 0 & 1 & 0 & 1 & \cdots & 0 & 1 \\ s_1(1) & c_1(1) & s_1(3) & c_1(3) & \cdots & s_1(11) & c_1(11) \\ s_2(1) & c_2(1) & s_2(3) & c_2(3) & \cdots & s_2(11) & c_2(11) \\ \vdots & & & & & & \\ s_{N-1}(1) & c_{N-1}(1) & s_{N-1}(3) & c_{N-1}(3) & \cdots & s_{N-1}(11) & c_{N-1}(11) \end{bmatrix} \tag{20}$$

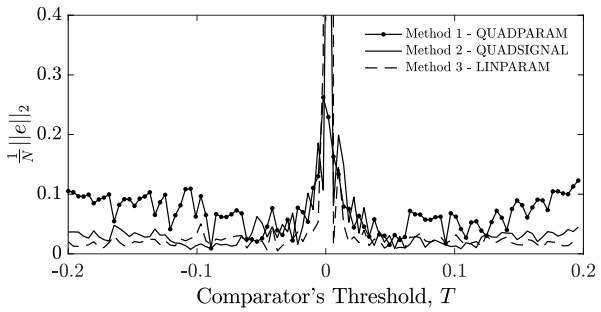

Fig. 7. No noise, no dither setup: normalized L^2-norm of the error sequences in estimating the signal with components listed in Table I, as a function of the comparator's threshold when $N = 2500$ samples. Points at $T = 0$ are removed because amplitude estimation is unfeasible in this case.

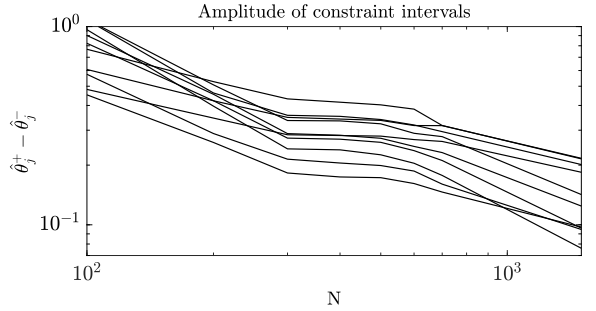

Fig. 8. Amplitude of the constraint intervals $\hat{\theta}_j^+ - \hat{\theta}_j^-$, $j = 1, \ldots, 2P$ defined in (18) and (12), as a function of N. The example with $P = 5$ and values listed in Table I is considered. By increasing N, asynchronous sampling results in shrinking of all constraint interval amplitudes.

threshold value and provide tighter bounds for the parameters to be estimated. In turn, this results in $\hat{\theta}_j^+$ approaching $\hat{\theta}_j^-$. When synchronous sampling is adopted, all graphs remain constant and independent on N.

B. No Noise, With Known Deterministic Dither Setup

1) Theory: If the amount of information at the comparator's output is too little, the estimation accuracy is low. As an example, if the input signal is constant or it rarely intercepts the threshold, $\mathbf{s}_q$ will mostly contain repeated binary information that may be insufficient for estimation purposes [46]. Similarly, if $\mathbf{s}_q$ is obtained by sampling synchronously a periodic sequence, its associated information will not increase when N increases, limiting the consistency of all estimators. This problem can be overcome by the addition of dither before quantization. A dither sequence can be sourced by a digital-to-analog converter or through an analog reference voltage, suitably processed by dedicated analog circuitry. Dither can be in the form of a noise sequence [7] or a deterministic sequence [47]. This latter case can also be solved with the presented methods.

When the effect of noise is not included in the model, according to (2), x_{qn} is equal to 1 if $s_n + d_n \leq T$, that is, $s_n \leq T - d_n$, where the rightmost term is a known value. Thus, the set of constraints must be modified as described in Section III-E. Define $\mathbf{D} = [d_0, d_1, \ldots, d_{N-1}]^T$, as the vector of dither samples. The application of method 1 provides

$$\hat{\Theta} = \arg\min_{\Theta} \frac{1}{N}(\mathbf{x}_q - \mathbf{H}\Theta)^T(\mathbf{x}_q - \mathbf{H}\Theta) \quad \text{s.t. } \operatorname{diag}(\mathbf{x}_q)\mathbf{H}\Theta \preccurlyeq (T - \mathbf{D}) \circ \mathbf{x}_q \tag{21}$$

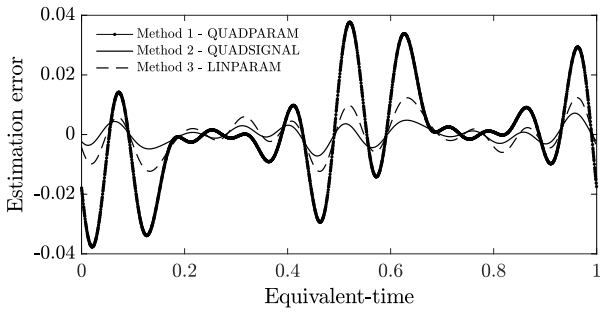

Fig. 9. No noise, sinusoidal dither setup: error in the estimation of the signal with components listed in Table I, when $N = 2500$ samples. Known dither $d_n = 0.5\sin(2\pi(\pi/7)n)$, $n = 0, \ldots, N-1$, is assumed. Results of all methods are shown when $T = -0.1643\ldots$

where $\circ$ indicates the Hadamard product between two matrices. Similarly, from (15), method 2 can be updated as follows:

$$\hat{\mathbf{Y}} = \arg\min_{\mathbf{Y}} \frac{1}{N}\mathbf{Y}^T\mathbf{Z}\mathbf{Y} \quad \text{s.t. } \mathbf{A}\mathbf{Y} \preccurlyeq \mathbf{Y}_D \tag{22}$$

where

$$\mathbf{Y}_D = \begin{bmatrix} \Theta_U \\ \mathbf{S}_D \end{bmatrix} \tag{23}$$

is an $(N+2P)\times 1$ vector, $\mathbf{S}_D = (T - \mathbf{D}) \circ \mathbf{x}_q$ is an $N \times 1$ vector, and

$$\mathbf{A} = \left[\begin{array}{c|c} \mathbf{I}_{2P} & \mathbf{0} \\ \hline \mathbf{0} & \operatorname{diag}(\mathbf{x}_q) \end{array}\right] \tag{24}$$

is an $(N + 2P) \times (N + 2P)$ matrix.

Method 3 must be modified such that for each $j = 1, \ldots, 2P$, the two following linear programming problems can be setup:

$$\hat{\theta}_j^+ = \arg\min_{\Theta} \theta_j \quad \text{s.t. } \operatorname{diag}(\mathbf{x}_q)\mathbf{H}\Theta \preccurlyeq (T - \mathbf{D}) \circ \mathbf{x}_q \tag{25}$$

and

$$\hat{\theta}_j^- = \arg\min_{\Theta} (-\theta_j) \quad \text{s.t. } \operatorname{diag}(\mathbf{x}_q)\mathbf{H}\Theta \preccurlyeq (T - \mathbf{D}) \circ \mathbf{x}_q \tag{26}$$

and by selecting, e.g., $\hat{\theta}_j = (1/2)(\hat{\theta}_j^+ + \hat{\theta}_j^-)$, $j = 1, \ldots, 2P$.

2) Simulation Results: The same example as in Section IV-A5 is considered in this section. As an example, the sinusoidal signal $d_n = 0.5\sin(2\pi(\pi/7)n)$, $n = 0, \ldots, N-1$, is used as a known dither sequence, throughout this article. The application of all methods provides the results shown in Figs. 9 and 10, to be compared with Figs. 6 and 7, respectively. As shown in Fig. 7, dither provides much more information available for the estimator that results in a much lower error norm and also allows estimation when $T = 0$.

C. Estimator Bias

The bias of estimator QUADSIGNAL is analyzed in this Section. First, Monte Carlo simulations were used to graph the norm of the bias in estimating each component of Θ, assuming dither with $d_n = 0.5\sin(2\pi(\pi/7)n + \phi)$, $n = 0, \ldots, N-1$, where ϕ is assumed as a uniform random variable in $[0, 2\pi)$.

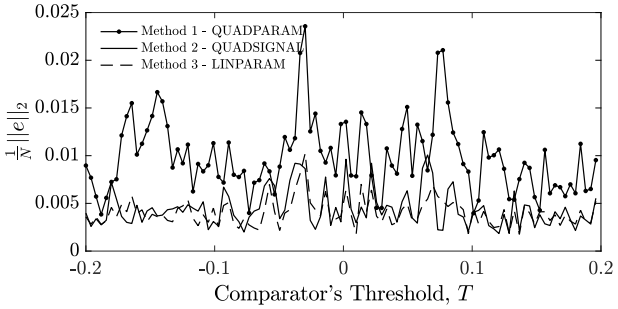

Fig. 10. No noise, sinusoidal dither setup: normalized L^2-norm of the error sequences in estimating the signal with components listed in Table I, as a function of the comparator's threshold when $N = 2500$ samples.

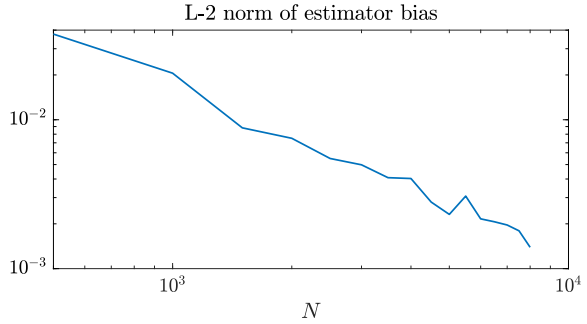

Fig. 11. No noise, sinusoidal dither setup: normalized L^2-norm of the error sequences in estimating the signal with components listed in Table I, using QUADSIGNAL, as a function of N.

The L^2-norm of the bias components obtained by averaging 10 data records associated with the signal with components listed in Table I is shown in Fig. 11, as a function of N. It can be seen that it decreases with N as $(1/N)$. This behavior can be explained as follows. If the constraints are not active, Θ can be chosen by the algorithm such that the cost function (12) approaches 0. For any θ_i in Θ, the sensitivity of the solution $\hat{s}_n = \mathbf{h}_n\Theta$ to variations of θ_i can be written as $\Delta\hat{s}_n = (\partial\hat{s}_n/\partial\theta_i)\Delta\theta_i = h_{ni}\Delta\theta_i$, where h_{ni} is the ith element of $\mathbf{h}_n$. Define ε as the distance of the signal point closest to threshold. When sampling is asynchronous, $\varepsilon \in O(N^{-1})$. Thus, $|\Delta\hat{s}_n| < \varepsilon$ or $|\Delta\theta_i| < (1/(|\partial\hat{s}_n/\partial\theta_i|))\varepsilon = (1/|h_{ni}|)\varepsilon \in O(N^{-1})$, as shown in Fig. 11.

D. Noise, With Known Deterministic Dither Setting

1) Theory: Additive noise may corrupt the input signal. Accordingly, $x_{qn} = Q(s_n + d_n + \eta_n)$, where the sequence η_n, $n = 0, \ldots, N-1$, represents the sequence of noise occurrences. By this redefinition, method 2 in (22) can be applied as is, assuming d_n known. Conversely, when applying method 1, because of the presence of noise, the constraints in (10) could result in an unfeasible solution. Thus, $\delta > 0$ can be seen as a guardbanding, tolerance value that can be set at the assumed maximum noise magnitude. Since, in practice, this value is not known, if δ is too small, running the solver can result in an unfeasible solution. If this occurs, δ can be increased until a feasible solution is found by running the solver on the same record of data. While also method 3 could be modified by the inclusion of a tolerance value when searching for a solution satisfying the constraints, a new method is introduced in Section IV-E1 that exploits the results presented in Section III-F.

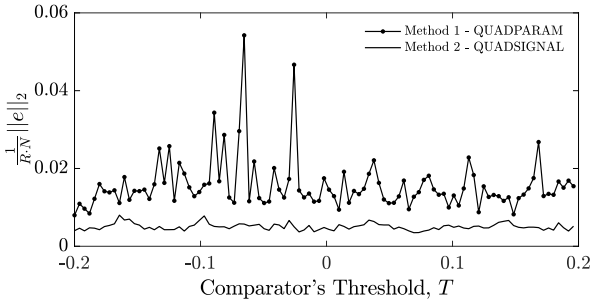

Fig. 12. Noise, sinusoidal dither setup: normalized L^2-norm of the error sequences in estimating the signal with components listed in Table I, as a function of the comparator's threshold when $N = 2500$ samples and $R = 20$ is the number of data records.

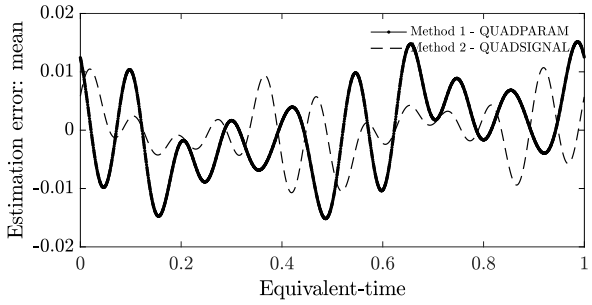

Fig. 13. Noise, sinusoidal dither setup: average error sequences in estimating the signal with components listed in Table I, when $N = 2500$ samples and $R = 20$ is the number of data records. Results of both methods are shown when $T = -0.1643\ldots$

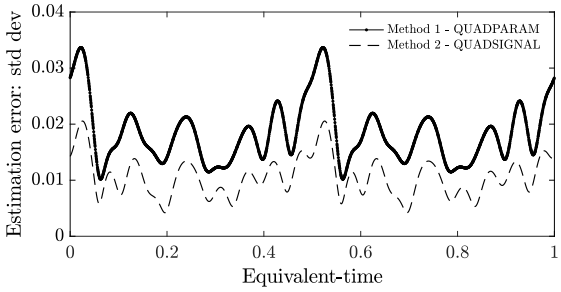

Fig. 14. Noise, sinusoidal dither setup: standard deviation of the error sequences in estimating the signal with components listed in Table I, when $N = 2500$ samples and $R = 20$ is the number of data records. Results of methods 1 and 2 are shown when $T = -0.1643\ldots$

2) Simulation Results: The same example as in Section IV-B2 is considered in this section. As an example, zero-mean additive Gaussian noise having standard deviation $\sigma = 0.01$ is added to the periodic signal in front of the comparator. The application of methods 1 and 2, assuming $\delta = 0.05$, provides the results shown in Figs. 12–15. By comparing Fig. 12 with Fig. 10, you can appreciate the regularizing effect of noise: with a slight increase in the overall error norm, peaks are partially smoothed in Fig. 12.

E. No Noise, Random Dither Setting

1) Theory: When random dither with known PDF is used to assist quantization at the comparator's input, constraints with boundaries l_j, u_j, $j \in \mathcal{S}$ can be obtained by the procedure described in Section III-F. Then, method 3 can be applied by

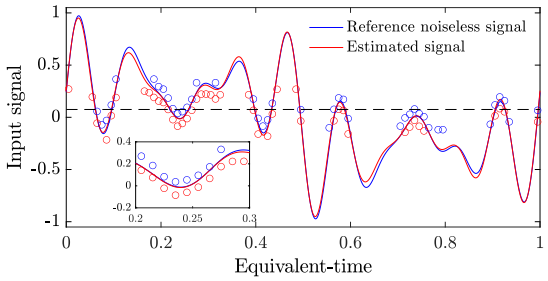

Fig. 15. Zero-mean Gaussian dither with $\sigma = 0.125$: original noiseless signal and signal reconstructed using Method 3. $N = 10^4$ samples are processed, assuming $T = 0.075$ shown using dashed lines; blue and red circles represent the values of the constraints calculated with $\epsilon = 0.01$ and $\alpha = 10^{-4}$. The inset shows an enlarged view. Observe that bounds appear close to T, within the reach of the random dither amplitude span in the order of $\pm 3\sigma$ about T.

solving the two following linear programming problem sets, for a total of $2P$ problems:

$$\hat{\theta}_j^+ = \arg\min_{\Theta} \ \theta_j \quad \text{s.t. } l_j < \overline{\mathbf{h}}_j \Theta < u_j, \quad j \in \mathcal{S} \tag{27}$$

and

$$\hat{\theta}_j^- = \arg\min_{\Theta} \ (-\theta_j) \quad \text{s.t. } l_j < \overline{\mathbf{h}}_j \Theta < u_j, \quad j \in \mathcal{S} \tag{28}$$

and by selecting, e.g., $\hat{\theta}_j = (1/2)(\hat{\theta}_j^+ + \hat{\theta}_j^-)$, $j = 1, \ldots, 2P$.

2) Simulation Results: Method 3 was simulated using 20 Monte Carlo records and zero-mean Gaussian dither with $\sigma = 0.125$. Results are shown in Fig. 15. The same example as in Section IV-B2 was considered with the simulation parameters set as listed in Fig. 15. Blue and red circles indicate the range of each constraint, calculated by (7). Based on these constraints, signal parameters are estimated using (27) and (28).

F. Statistical Performance

The L^2-norms of the variance and mean square errors (MSEs) of LINPARAM based on Gaussian random dither to build equivalent constraints are evaluated using a Monte Carlo method. Results based on simulation parameters listed in Table I are graphed in Fig. 16(a) along with the L^2-norm of the Cramér–Rao lower bound (CRLB) applicable to this case. The CRLB was computed by using its expression published in [6, eq. (55)]. It can be observed that the loss of statistical efficiency is moderate. The estimator variance and MSE associated with each component in the vector of parameters are shown in Fig. 16(b), together with the corresponding CRLB, when $N = 6 \times 10^3$.

Observe that if noise corrupts the samples in addition to dither, two cases apply: if the noise PDF is known, its effects can be aggregated to those of the dither and can be modeled to retain estimation accuracy; alternatively, its effects remain unmodeled and LINPARAM cannot be applied as is, since noise could invalidate the check performed by the algorithm on the solution feasibility. In this latter case, a tolerance parameter could be defined as described in Section III-G or α in (5) can be modified until feasibility is achieved. This approach is not further discussed in this article.

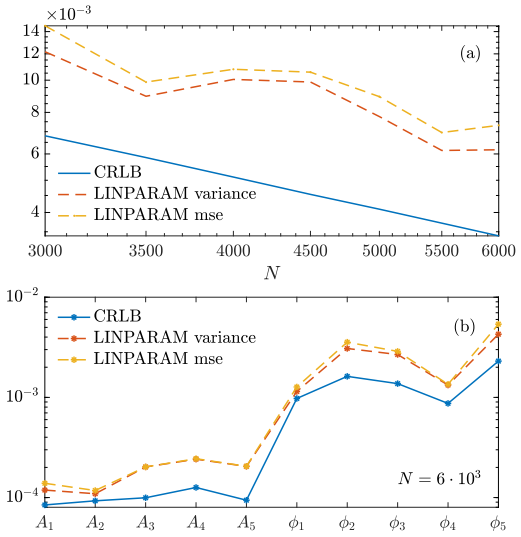

Fig. 16. Zero-mean Gaussian dither with $\sigma = 0.3$: signal reconstructed using method 3 (LINPARAM) based on the random dither constraints setup as illustrated in Section III-F. (a) CRLB, estimator variance, and MSE as a function of N and associated with (b) each of the ten signal components. $T = -0.16435\ldots$ is assumed, with $\epsilon = 0.02$ and $\alpha = 10^{-3}$.

TABLE II

PROPERTIES OF THE METHODS DESCRIBED IN THIS ARTICLE: * IF THE NOISE PDF IS KNOWN, NOISE CAN BE REGARDED AS BEING ADDITIONAL STOCHASTIC DITHER

Method	Stochastic dither	Deterministic dither	Synch/Asynch	Noise
QUADSIGNAL	-	✓	✓	large/moderate SNR
QUADPARAM	-	✓	✓	large SNR
LINPARAM	✓	✓	✓	*
BQBE [34]	✓	-	✓	*

V. MONTE CARLO COMPARISON OF ALL METHODS

The estimation performance of the three methods proposed in this article was determined by Monte Carlo simulations based on 20 records. All possible problem settings listed in Table II were considered. Simulations were divided into two subgroups according to the type of applied dither signal: stochastic, that is, zero-mean Gaussian noise with standard deviation $\sigma = 0.3$ and deterministic, given by $d_n = 0.5 \sin(2\pi(\pi/7)n)$, $n = 0, \ldots, N-1$. Observe that the dither prior information differs significantly in the two cases. Deterministic dithering implies that the amplitude of each dither sample is known, and stochastic dithering only assumes the dither PDF to be known.

Results assuming deterministic and stochastic dithering are shown in Fig. 17(a) and (b), respectively. Each bar in Fig. 17 represents the mean value of the root-mean-square error (RMSE), calculated over all data records. A 3-bit code was assigned to each setting, where, from the leftmost to the rightmost positions, each bitcode 0/1 represents asynchronous/synchronous sampling, absence/addition of dithering, and absence/addition of noise. In this latter case, zero-mean Gaussian noise with standard deviation 0.01 was added prior to quantization. The generated signal is the same signal used in the simulations illustrated throughout this article, with $N = 5 \times 10^3$. In the asynchronous case, $\lambda = 0.011323235562$ was assumed, while $\lambda = (99/N)$, in the synchronous case.

Observe that the LINPARAM method, under the deterministic dither setting, does not support the addition of noise.

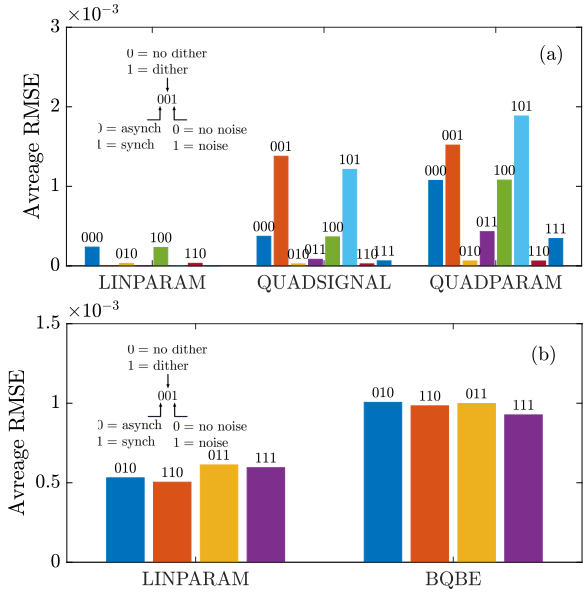

Fig. 17. Monte Carlo comparison of all methods under the various estimation settings, coded using the displayed 3-bit code. Shown is the RMSE averaged over $R = 20$ records of data, each assuming the periodic signal whose parameters are shown in Table I: (a) and (b) Usage of sinusoidal deterministic dither, with 0.5 peak amplitude, and zero-mean Gaussian stochastic dither, having standard deviation 0.3, respectively. The LINPARAM method in (a) does not support the addition of additive noise. It outperforms the other methods under the settings in which it can be applied. When additive noise affects data prior to quantization, the QUADSIGNAL method works at best; in (b), the comparison is made between LINPARAM and the BQBE proposed in [34]. The former has a better performance at the expense of increased computational burden.

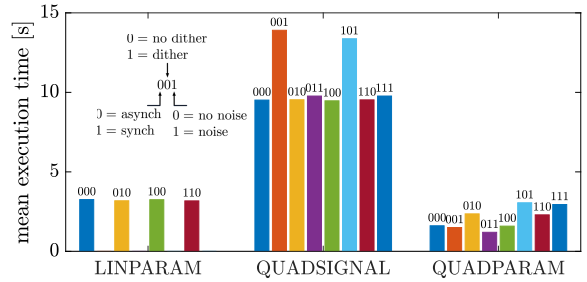

Fig. 18. Monte Carlo comparison of the mean execution times under the same estimation problem settings, adopted in Fig. 17, and coded using the displayed 3-bit code. Results are based on $R = 20$ data records, each obtained on a double-core i7 computer.

At the same time, when deterministic dithering is not applied, LINPARAM can support the presence of noise, if noise can be regarded as a stochastic dither, and thus, its PDF is assumed known. Thus, only four bars are shown in Fig. 17(a).

LINPARAM and QUADSIGNAL provide similar results, while QUADPARAM provides worse results under the settings 000 and 010 and under all noisy settings XX1, where X is either 0 or 1. However, LINPARAM is much faster than QUADSIGNAL, as shown in Fig. 18, which reports average processing times under the same settings. These were determined empirically on a dual-core i7-based computer.

Fig. 17(b) shows the average RMSE associated with the usage of LINPARAM under the stochastic dithering setting. Since QUADPARAM and QUADSIGNAL do not support this setting, the comparison was made with an applicable estimator, the binary quantile-based estimator (BQBE) presented in [34].

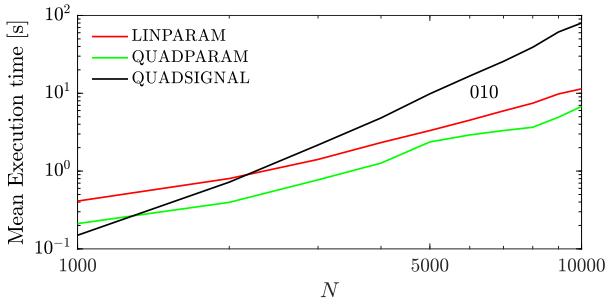

Fig. 19. No noise, known sinusoidal dither setup: mean values of the estimators' execution times in seconds, as a function of the record length N. Results of all methods are shown, under the setting 010 when using a double-core i7 CPU. Sinusoidal dither amplitude is equal to 0.5.

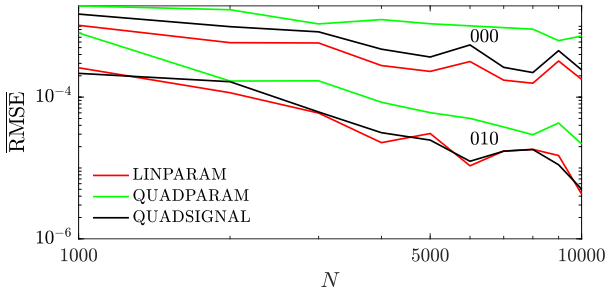

Fig. 20. No noise, known sinusoidal dither setup: average RMSE of the error sequences in estimating the signal with components listed in Table I, as a function of the record length N, averaged over $R = 10$ Monte Carlo records. Sinusoidal dither amplitude is equal to 0.5. Results of settings coded as 000 and 010 are shown when $T = -0.1643\ldots$ group of graphs refers to the usage of the estimation techniques listed in the legend.

A. Effect of Record Length

The average of the RMSE of the signal reconstruction error associated with all methods as a function of the record length N is shown in Fig. 20, assuming a sinusoidal dither sequence. The same example as in Section IV-D2 is considered. Monte Carlo results are based on $R = 10$ records of data. Observe that LINPARAM and QUADPARAM outperform QUADSIGNAL. However, the average execution times of QUADPARAM are about one order of magnitude larger on a dual-core i7-based computer, as shown as a function of N, in Fig. 19.

VI. Experimental Results

An area where binary quantization could result in simpler acquisition hardware than more complex multibit resolution ADCs is that of high-frequency signal acquisition. Accordingly, experimental data were obtained by generating a two-tone signal using a vector signal generator and by collecting samples using a 4-GHz, 10-bit, 40-GS/s digital sampling oscilloscope. Two tones are generated with nominal frequencies equal to $f_1 = 1.195$ GHz and $f_2 = 1.205$ GHz. Amplitudes of signal samples ranged in $[-0.3156, 0.3269]$ V. The estimated signal spectrum, based on the full record of $N = 100\,002$ samples, collected by the 10-bit resolution digital storage oscilloscope (DSO), is plotted in Fig. 21. It can be observed the presence of several tones due to signal distortion and of colored wideband noise. Data were quantized via software using a threshold $T = 0.239861832917778$ V. The signal mean value was preliminary filtered. The one-bit time series was then processed as described in this article.

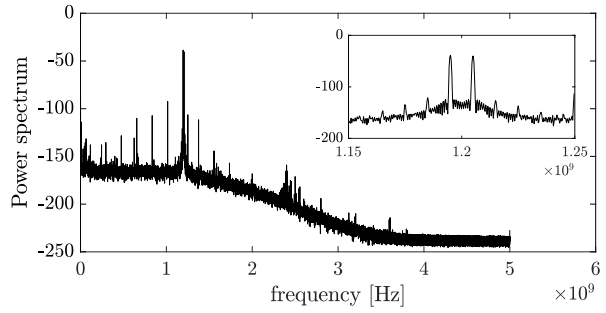

Fig. 21. Estimated spectrum of a two-tone signal with frequencies 1.195 and 1.205 GHz, generated by a vector signal generator and acquired by a 4-GHz DSO. The estimation is based on $N = 100\,002$ samples. The inset shows the two components in an expanded frequency interval. Notice both the narrowband distortion components and the colored wideband noise.

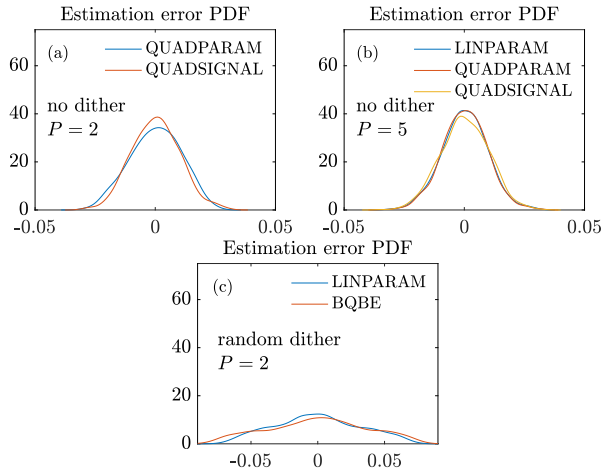

Fig. 22. Experimental data of the two-tone signal with spectrum shown in Fig. 21: estimation of the error PDF based on a kernel estimator. Errors are calculated as the difference between the full-resolution signal and the estimated sequence based on $N = 900$ binary samples. Plots are associated with the usage of (a) two and (b) three estimation methods based on $P = 2$ and $P = 5$ sinusoidal components, respectively. The more complex model results in a reduced dispersion of the estimation error. (c) Usage of LINPARAM with $P = 2$ under the setting including zero-mean Gaussian stochastic dither with $\sigma = 0.2$. It is also shown the error performance of the BQBE proposed in [34].

First, a model with $P = 2$ was set up, by assuming f_1 and f_2 known. $N = 900$ samples were processed by two of the three methods. The presence of unmodeled narrowband components and wideband noise in the data made LINPARAM inapplicable. After parametric estimation, the error sequences were calculated as the difference between the reconstructed and the full-resolution signal. The associated PDFs were then estimated using a kernel-based approach. The results are shown in Fig. 22(a) when using QUADPARAM and QUADSIGNAL. By increasing the model order to $P = 5$ with components having frequencies $f_3 = 1.2500$, $f_4 = 1.1015$, and $f_5 = 1.3750$ GHz, LINPARAM became applicable. The related error PDFs are shown in Fig. 22(b). A lower error dispersion results. However, the choice $P = 5$ requires prior knowledge about the signal distortion that might not be available to the user.

Finally, stochastic dither was used in generating binary quantization, through simulation. Gaussian dither was used, having zero-mean and $\sigma = 0.2$. The application of LINPARAM, as explained in Section IV-E2, when assuming $P = 2$ and $N = 15 \times 10^3$ produced the error PDF shown in Fig. 22(c). These results are characterized by a larger estimation error variance with respect to errors in Fig. 22(a) and (b).

VII. User-Oriented Approach

From a user perspective, the choice of which method to use among those described in this article can initially be based on the presence or absence of noise. If the SNR is large, LINPARAM can possibly be considered as the best choice in terms of computational complexity and accuracy of results. Even though it assumes a noiseless sequence, it can account for the presence of noise, if noise samples do not invalidate the constraints, as shown in Section VI. Also, QUADPARAM and QUADSIGNAL can be used. However, QUADPARAM is characterized by a larger RMSE and QUADSIGNAL requires higher computational complexity.

If the SNR is low, LINPARAM can no longer be applied. If the number of samples is sufficiently small, e.g., less than 10^4, QUADSIGNAL provides the best results. Alternatively, QUADPARAM becomes the only option. Moreover, if the noise PDF is known, LINPARAM with stochastic constraints, as described in Section IV-E1, becomes applicable and a possible alternative to the usage of BQBE [34].

Similar reasoning applies in case of deterministic dither with known samples. When the SNR is large, LINPARAM and QUADSIGNAL are the best choices, while QUADPARAM provides worse results. When the SNR decreases, QUADSIGNAL exhibits the best compromise between complexity and estimation accuracy. Moreover, the usage of stochastic instead of deterministic dither is equivalent to the case of wideband noise with known PDF.

Finally, if sampling can be made asynchronous, an increase in N may result in tighter constraints and thus in feasible regions of reduced size, as shown in Fig. 3(a). Conversely, if sampling is synchronous, increase in estimation accuracy can be obtained through dithering or by increasing N, in case LINPARAM with stochastic dithering is used. A list of the estimators' applicability under the various problem settings is shown in Table II.

A. Limitations of the Presented Estimation Methods

Several assumptions were made throughout this article to support the construction of the presented estimators. Estimation is enabled even after one-bit severe quantization in any of the considered settings, by the assumption that signal sampling is asynchronous. In fact, when periodic signals are sampled synchronously, the sample sequence becomes periodic and parameters can be recovered only if deterministic or stochastic dither is employed. However, if deterministic dither is obtained by synchronous sampling of a periodic signal, then chaotic patterns can arise if the signal and dither frequencies are not synchronized. Stochastic dither can break the periodicity of the synchronous samples signal, but it requires knowledge of its PDF to ease estimation or prior information to be used for its estimation [26].

When dither is not used, signal estimation is only based on the estimation of times associated with the signal crossing

the threshold. As discussed in Section III-H, the value of T plays a significant role in determining the number of crossings and thus the number of independent equations to be used for estimation of the parameters of the signal components. The estimation will still be possible when asynchronous sampling is adopted and the number of samples goes to infinity since the constraints reduce the size of the feasible region, as shown in Fig. 3. Even unconstrained estimation will still be possible in this case if a single component is assumed, as shown in [39].

Frequencies of processed components are assumed known in this article. In practice, this might not be a severe limitation when signals are generated by the user for, e.g., testing purposes. Conversely, if no prior knowledge about the frequency of signal components is available, but the number of components is known, the discrete-time Fourier transform of the one-bit sequence can be used to detect the most powerful components. These can be processed one-by-one by the estimators described in this article, as done, for instance, in [37].

Signal recovery is based in this article on the knowledge of the signal structure, e.g., a linear in the parameter sequence. If this hypothesis is removed and signals are allowed not to be bound to a defined model structure, the presented procedures will not be applicable. Finally, observe that while knowledge of the wideband noise PDF may be incorporated in the estimators to improve their accuracy, some of the techniques presented in this article allow estimation also without this knowledge.

VIII. Conclusion

A framework was presented in this article to estimate the amplitudes and phases of the sinusoidal components in a periodic signal, based on binary quantized data. The analyzed problem settings include the possible presence of stochastic or deterministic dithering, the possibility to sample signals synchronously or asynchronously, and the possible presence of additive noise in quantizing signals. Three estimation methods are illustrated. All methods are based on constrained optimization. They exhibit complementary properties in terms of accuracy, numerical complexity, and capability to account for the possible presence of dither and noise.

Several application examples were described. Usage of experimental data validates the described estimators and shows their application limits in the presence of unmodeled signal components.

References

[1] R. Pintelon and J. Schoukens, "Robust identification of transfer functions in the s- and z-domains," *IEEE Trans. Instrum. Meas.*, vol. 39, no. 4, pp. 565–573, Aug. 1990.

[2] G. Barchi, D. Fontanelli, D. Macii, and D. Petri, "On the accuracy of phasor angle measurements in power networks," *IEEE Trans. Instrum. Meas.*, vol. 64, no. 5, pp. 1129–1139, May 2015.

[3] E. Masry, "The reconstruction of analog signals from the sign of their noisy samples," *IEEE Trans. Inf. Theory*, vol. IT-27, no. 6, pp. 735–745, Nov. 1981.

[4] R. E. Curry, *Estimation and Control With Quantized Measurements*. Cambridge, MA, USA: The Massachusetts Institute of Technology, 1970.

[5] A. Ribeiro and G. B. Giannakis, "Bandwidth-constrained distributed estimation for wireless sensor networks—Part I: Gaussian case," *IEEE Trans. Signal Process.*, vol. 54, no. 3, pp. 1131–1143, Mar. 2006.

[6] A. Ribeiro and G.-B. phantom, "Bandwidth-constrained distributed estimation for wireless sensor networks—Part II: Unknown probability density function," *IEEE Trans. Signal Process.*, vol. 54, no. 7, pp. 2784–2796, Jul. 2006.

[7] P. Carbone, "Quantitative criteria for the design of dither-based quantizing systems," *IEEE Trans. Instrum. Meas.*, vol. 46, no. 3, pp. 656–659, Jun. 1997.

[8] O. Dabeer and A. Karnik, "Signal parameter estimation using 1-bit dithered quantization," *IEEE Trans. Inf. Theory*, vol. 52, no. 12, pp. 5389–5405, Dec. 2006.

[9] M. S. Stein, S. Bar, J. A. Nossek, and J. Tabrikian, "Performance analysis for channel estimation with 1-bit ADC and unknown quantization threshold," *IEEE Trans. Signal Process.*, vol. 66, no. 10, pp. 2557–2571, May 2018.

[10] A. Host-Madsen and P. Handel, "Effects of sampling and quantization on single-tone frequency estimation," *IEEE Trans. Signal Process.*, vol. 48, no. 3, pp. 650–662, Mar. 2000.

[11] C. Gianelli, L. Xu, J. Li, and P. Stoica, "One-bit compressive sampling with time-varying thresholds: Maximum likelihood and the Cramér-Rao bound," in *Proc. 50th Asilomar Conf. Signals, Syst. Comput.*, Nov. 2016, pp. 399–403.

[12] C. Gianelli, L. Xu, J. Li, and P. Stoica, "One-bit compressive sampling with time-varying thresholds for multiple sinusoids," in *Proc. IEEE 7th Int. Workshop Comput. Adv. Multi-Sensor Adapt. Process. (CAMSAP)*, Dec. 2017, pp. 1–5.

[13] X. Huang and B. Liao, "One-bit MUSIC," *IEEE Signal Process. Lett.*, vol. 26, no. 7, pp. 961–965, Jul. 2019.

[14] O. Orhan, E. Erkip, and S. Rangan, "Low power analog-to-digital conversion in millimeter wave systems: Impact of resolution and bandwidth on performance," in *Proc. Inf. Theory Appl. Workshop (ITA)*, Feb. 2015, pp. 191–198.

[15] J. Li, M. M. Naghsh, S. J. Zahabi, and M. Modarres-Hashemi, "Compressive radar sensing via one-bit sampling with time-varying thresholds," in *Proc. 50th Asilomar Conf. Signals, Syst. Comput.*, Nov. 2016, pp. 1164–1168.

[16] Z. Liu, C. Li, and Z. Zhang, "One-bit recursive least-squares algorithm with application to distributed target localization," *IEEE Trans. Aerosp. Electron. Syst.*, vol. 55, no. 5, pp. 2296–2313, Oct. 2019.

[17] O. Bar-Shalom and A. J. Weiss, "DOA estimation using one-bit quantized measurements," *IEEE Trans. Aerosp. Electron. Syst.*, vol. 38, no. 3, pp. 868–884, Jul. 2002.

[18] A. Ai, A. Lapanowski, Y. Plan, and R. Vershynin, "One-bit compressed sensing with non-Gaussian measurements," *Linear Algebra Appl.*, vol. 441, pp. 222–239, Jan. 2014.

[19] H. Zayyani, M. Korki, and F. Marvasti, "A distributed 1-bit compressed sensing algorithm robust to impulsive noise," *IEEE Commun. Lett.*, vol. 20, no. 6, pp. 1132–1135, Jun. 2016.

[20] K. Knudson, R. Saab, and R. Ward, "One-bit compressive sensing with norm estimation," *IEEE Trans. Inf. Theory*, vol. 62, no. 2, pp. 2748–2758, May 2016.

[21] L. Chen, X. Tang, A. Sanyal, Y. Yoon, J. Cong, and N. Sun, "A 0.7-V 0.6-μW 100-kS/s low-power SAR ADC with statistical estimation-based noise reduction," *IEEE J. Solid-State Circuits*, vol. 52, no. 5, pp. 1388–1398, May 2017.

[22] A. Jayaraj, S. T. Chandrasekaran, A. Ganesh, I. Banerjee, and A. Sanyal, "Maximum likelihood estimation-based SAR ADC," *IEEE Trans. Circuits Syst. II, Exp. Briefs*, vol. 66, no. 8, pp. 1311–1315, Aug. 2019.

[23] N. S. C. Tang, "Statistical estimation-based noise reduction technique for low power successive approximation register analog-to-digital converters," U.S. Patent US9 774 339 B2, May 9, 2015. [Online]. Available: https://patents.google.com/patent/US9774339B2/en

[24] Z. Lei and Z. Xiaolin, "Mismatch suppression and noise reduction for SAR-ADC with Bayes estimation method," *Anal. Integr. Circuits Signal Process.*, vol. 102, no. 2, pp. 379–388, Jan. 2020.

[25] M. Stein, "Signal parameter estimation with 1-bit ADC performance—Bounds, methods and system design," Ph.D. dissertation, Dept. Fakultät für Elektrotechnik und Informationstechnik, Inst. Circuit Theory Signal Process. Technische Universität München, Munich, Germany, 2016.

[26] L. Y. Wang, G. G. Yin, J.-F. Zhang, and Y. Zhao, *System Identification With Quantized Observations*. Boston, MA, USA: Birkhäuser, 2010, doi: 10.1007/978-0-8176-4956-2.

[27] Y. Wang, Y. Zhao, J.-F. Zhang, and J. Guo, "A unified identification algorithm of FIR systems based on binary observations with time-varying thresholds," *Automatica*, vol. 135, Jan. 2022, Art. no. 109990.

[28] M. Saito *et al.* (2022). *Noise-Assisted Nonlinear Estimation of a One-Bit ADC Output and its Application to a Multi-Antenna Receiver*. [Online]. Available: https://www.techrxiv.org/articles/preprint/Noise-assisted_nonlinear_estimation_of_a_one-bit_ADC_output_and_its_application_to_a_multi-antenna_receiver/19446947

[29] P. Carbone, J. Schoukens, and A. D. Angelis, "One-bit system identification," *IFAC-PapersOnLine*, vol. 54, no. 7, pp. 571–576, 2021.

[30] O. T. Demir and E. Bjornson, "The Bussgang decomposition of nonlinear systems: Basic theory and MIMO extensions [lecture notes]," *IEEE Signal Process. Mag.*, vol. 38, no. 1, pp. 131–136, Jan. 2021.

[31] M. Milanese and A. Vicino, "Optimal estimation theory for dynamic systems with set membership uncertainty," *Automatica*, vol. 27, no. 6, pp. 997–1009, Nov. 1991.

[32] E. J. Candès and T. Tao, "Decoding by linear programming," *IEEE Trans. Inf. Theory*, vol. 51, no. 12, pp. 4203–4215, Dec. 2005.

[33] K. Takahashi, R. Roberts, Z. Jiang, and B. Memarzadeh, "Statistical evaluation of Signal-to-Noise ratio and timing jitter in equivalent-time sampling signals," *IEEE Trans. Instrum. Meas.*, vol. 70, pp. 1–4, 2021.

[34] P. Carbone, J. Schoukens, and A. Moschitta, "Quick estimation of periodic signal parameters from 1-Bit measurements," *IEEE Trans. Instrum. Meas.*, vol. 69, no. 2, pp. 339–353, Feb. 2020.

[35] R. Graham, *Concrete Mathematics: A Foundation for Computer Science*. Reading, MA, USA: Addison-Wesley, 1994.

[36] S. Epp, *Discrete Mathematics With Applications*. Belmont, CA, USA: Thomson-Brooks/Cole, 2004.

[37] P. Carbone, A. D. Angelis, F. Santoni, and A. Moschitta, "Measurement of the parameters of multiple sinusoids based on binary data," *IEEE Trans. Instrum. Meas.*, vol. 70, pp. 1–10, 2021.

[38] J. P. Boyd, "Computing the zeros, maxima and inflection points of chebyshev, legendre and Fourier series: Solving transcendental equations by spectral interpolation and polynomial rootfinding," *J. Eng. Math.*, vol. 56, no. 3, pp. 203–219, Nov. 2006.

[39] P. Carbone, J. Schoukens, A. De Angelis, F. Santoni, A. Comuniello, and A. Moschitta, "One-bit sine-fit," *IEEE Trans. Instrum. Meas.*, vol. 70, pp. 1–12, 2021.

[40] R. H. Byrd, J. C. Gilbert, and J. Nocedal, "A trust region method based on interior point techniques for nonlinear programming," *Math. Program.*, vol. 89, no. 1, pp. 149–185, Nov. 2000.

[41] R. A. Waltz, J. L. Morales, J. Nocedal, and D. Orban, "An interior algorithm for nonlinear optimization that combines line search and trust region steps," *Math. Program.*, vol. 107, no. 3, pp. 391–408, Nov. 2005.

[42] J. Wang and Q. Zhang, "Identification of FIR systems based on quantized output measurements: A quadratic programming-based method," *IEEE Trans. Autom. Control*, vol. 60, no. 5, pp. 1439–1444, May 2015.

[43] K. Konishi, "A robust SDP approach to system identification with roughly quantized data," in *Proc. IEEE Int. Conf. Syst., Man Cybern.*, San Antonio, TX, USA, Oct. 2009, pp. 2800–2805.

[44] P. Gill, *Practical Optimization*. London, U.K.: Academic, 1981.

[45] J. Marklof, S. O'Keefe, and S. Zelditch, "Weyl's law and quantum ergodicity for maps with divided phase space (with an appendix converse quantum ergodicity)," *Nonlinearity*, vol. 18, no. 1, pp. 277–304, Oct. 2004.

[46] A. Moschitta, J. Schoukens, and P. Carbone, "Information and statistical efficiency when quantizing noisy DC values," *IEEE Trans. Instrum. Meas.*, vol. 64, no. 2, pp. 308–317, Feb. 2015.

[47] P. Carbone, J. Schoukens, A. De Angelis, and A. Moschitta, "A 1.5-bit DFT analyzer," *IEEE Trans. Instrum. Meas.*, vol. 69, no. 10, pp. 8590–8599, Apr. 2020.

Paolo Carbone (Fellow, IEEE) received the master's and Ph.D. degrees from the University of Padova, Padua, Italy, in 1990 and 1994, respectively.

From 1994 to 1997, he was a Researcher with the Third University of Rome, Rome, Italy. From 1997 to 2002, he was first a Researcher and then an Associate Professor with the University of Perugia, Perugia, Italy. Since 2002, he has been a Full Professor with the University of Perugia, where he teaches courses in instrumentation and measurement and in statistical signal processing. He has been involved in various research projects, sponsored by private and public funds. He has authored or coauthored more than 200 papers, appeared in international journals and conference proceedings.

Dr. Carbone was the President of the IEEE Systems Council from 2016 to 2017. Since 2018, he has been the Editor-in-Chief of the journal *Measurement*.

Johan Schoukens (Fellow, IEEE) received the master's degree in electrical engineering, the Ph.D. degree in engineering sciences, and the Geaggregeerde voor het Hoger Onderwijs degree from Vrije Universiteit Brussel (VUB), Brussels, Belgium, in 1980, 1985, and 1991, respectively, the Doctor Honoris Causa degree from the Budapest University of Technology and Economics, Budapest, Hungary, in 2011, and the Doctor of Science from the University of Warwick, Coventry, U.K., in 2014.

From 1981 to 2000, he was a Researcher at VUB with a grant from the Belgian National Fund for Scientific Research. He was a full-time Professor in electrical engineering with VUB until 2018. Since 2018, he has been an Emeritus Professor at the Department INDI, VUB, and a member of the Department of Electrical Engineering, Eindhoven University of Technology, Eindhoven, The Netherlands. From 2009 to 2016, he was a Visiting Professor with the Department of Computer Sciences, Katholieke Universiteit Leuven, Leuven, Belgium. Since 2013, he has been an Honorary Professor with the University of Warwick. His main research interests include system identification, signal processing, and measurement techniques.

Dr. Schoukens has been a member of the Royal Flemish Academy of Belgium for Sciences and the Arts since 2010. He was a recipient of the 2002 Andrew R. Chi Best Paper Award of the IEEE TRANSACTIONS ON INSTRUMENTATION AND MEASUREMENT, the 2002 Society Distinguished Service Award from the IEEE Instrumentation and Measurement Society, and the 2007 Belgian Francqui Chair at the Université Libre de Bruxelles, Belgium. In 2020, he received from the IEEE Instrumentation and Measurement Society the Gold Medal for recognition as the Most Published Author of All Time in the Transactions on Instrumentation and Measurement.

Alessio De Angelis (Member, IEEE) received the Ph.D. degree in information engineering from the University of Perugia, Perugia, Italy, in 2009.

From 2010 to 2013, he was a Researcher with the Signal Processing Laboratory, KTH Royal Institute of Technology, Stockholm, Sweden. Since July 2013, he has been with the Department of Engineering, University of Perugia, where he became an Associate Professor in May 2018. His research interests include instrumentation and measurement, positioning systems (using magnetic field and ultrasound), statistical signal processing, and battery measurement and modeling.

Dr. De Angelis has been serving as an Associate Editor for IEEE TRANSACTIONS ON INSTRUMENTATION AND MEASUREMENT since 2019.

Antonio Moschitta (Member, IEEE) received the Ph.D. degree from the University of Perugia, Perugia, Italy, in 2002.

He is currently an Associate Professor with the University of Perugia. He is the author or coauthor of more than 120 papers, appearing in international journals or conference proceedings. His research interests include power quality, A/D, D/A, time-to-digital conversion, short-range positioning, and estimation theory.

Francesco Santoni (Member, IEEE) received the master's degree in physics from the University of Perugia, Perugia, Italy, in 2010, and the Ph.D. degree in electronic engineering from the University of Roma "Tor Vergata," Rome, Italy, in 2015.

He held a post-doctoral position at the University of Roma "Tor Vergata" from 2015 to 2017, where his research work was mainly focused on mathematical models of charge transport in organic semiconductors and simulations of organic electronic devices. In May 2017, he started working at the Department of Engineering, University of Perugia, as a Post-Doctor, where he became a Researcher in 2022. He is currently researching on magnetic positioning systems, battery management systems, and signal analysis.

Open Access funding provided by 'Università degli Studi di Perugia' within the CRUI CARE Agreement